Residual Stress and Pop-Out Simulation for TSVs and Contacts in Via-Middle Process

Can Rao, Tongqing Wang, Yarui Peng, *Student Member, IEEE*, Jie Cheng, Yuhong Liu, Sung Kyu Lim, *Senior Member, IEEE*, and Xinchun Lu

***Abstract*—In the via-middle process of 3-D integrated circuit manufacturing, through-silicon via (TSV) annealing causes mechanical stress not only to its surrounding structures, including liner and landing pad, but also the contacts nearby. This process may result in a noticeable pop-out in TSVs and/or contacts, thus complicating the subsequent chemical mechanical polishing (CMP). In addition, residual stress may cause delamination or crack. In this paper, we conducted detailed simulations of the residual stress and pop-out mechanisms for TSVs and neighboring contacts. Our primary focus was on the interplay of TSV-induced and contact-induced stresses and their combined impact on pop-out height. In addition, we conducted a sensitivity analysis of key parameters, including distance, plasticity, annealing temperature, and the distribution of neighboring contacts. This paper showed that these parameters notably affect the stress and the pop-out of TSVs and contacts. This in turn is expected to complicate the subsequent CMP steps. Finally, we applied the linear superposition method to predict stress and validated its accuracy by comparing the results with finite element analysis simulation. The results of the comparison demonstrated that the superposition method was accurate. Therefore, it could be used to predict the stress for full-chip design.**

***Index Terms*—Through-silicon via, chemical mechanical planarization, residual stress, pop-out.**

I. Introduction

IN THREE-DIMENSIONAL (3D) integrated circuit (IC) manufacturing, feature size is continuously decreasing while the size of silicon wafers has been increasing, from 150 mm and 200 mm, to 300 mm and 450 mm [1], [2]. However, the chip scaling will soon face the physical limitation, and this calls for the intensively investigated concept of through-silicon via (TSV). TSV fabrication is an effective approach to enable growing products in the z-direction [3], [4]. It mainly includes the following steps: photolithography, via etching, deposition of oxide liner/diffusion barrier/copper seed, electroplating, annealing, chemical mechanical planarization (CMP), and backside reveal [5]–[11]. During thermal annealing, a significant thermal expansion mismatch occurs and leads to thermo-mechanical stress. This is due to several reasons, the different coefficients of thermal expansion (CTE) of Cu, W, and Si, which result in the generation of a residual stress in TSVs or in the contacts of nearby devices [12], or the dislocation motion and temperature non-uniformity [13]. As TSVs and device contacts are constrained by the surrounding Si substrate, they will primarily expand in the vertical z-direction, and a pop-out phenomenon will eventually occur. This is a major issue, and may induce interfacial delamination and wafer warpage. Pop-out is becoming one of the biggest manufacturing challenges in 3D ICs [14], [15].

Many researchers have performed experiments to study the impact of annealing conditions, Cu crystal structures, Cu electroplating steps, and other factors on TSVs [14]–[16]. Simulations have been conducted to understand the influence of Cu grain growth, Cu overburden layer, or different annealing conditions on TSV [17], [18]. TSV pop-out is responsible for the damage of Cu metal and ultra-low-k (ULK) layers according to Tsai *et al.* [5]. Olmen *et al.* [19] studied TSV pop-out after the annealing process and observed crack formation in the back end of line (BEOL) layers. However, these studies did not focus on the co-simulation of TSVs and contacts.

Among various TSV fabrication processes, the via-middle approach is the most popular option and allows for larger flexibility in design [20]. However, it has a serious issue related to TSVs, contacts, and CMP, which is shown in Fig. 1. The CMP process in the front side of TSV will touch the TSV and the contact. CMP is used for ultra-large scale integration (ULSI) manufacturing because it enables the production of smaller ICs, extends the productivity of lithography by reducing the diffuse reflection, and helps reduce defects as well as increase IC yield [21], [22]. After the CMP process, if there is any residual stress at the interface between different layers or inside the material, it will be much easier for a crack to form and grow. Pop-out will also affect the force distribution on the wafer and cause a stress concentration around the TSV or a nearby contact. Both conditions result in more defects and reduce the IC yield. Therefore, it is necessary to investigate and resolve these issues.

Manuscript received March 9, 2017; accepted March 23, 2017. Date of publication March 28, 2017; date of current version May 3, 2017. This work was supported in part by the Science Fund for Creative Research Groups under Grant 51321092, in part by the National Natural Science Foundation of China under Grant 91323302, Grant 51405511, and Grant 21606207, and in part by the National Basic Research Program of China under Grant 2015CB057203. *(Corresponding authors: Sung Kyu Lim; Xinchun Lu.)*

C. Rao, T. Wang, J. Cheng, Y. Liu, and X. Lu are with the State Key Laboratory of Tribology, Tsinghua University, Beijing 100084, China (e-mail: raoc13@mails.tsinghua.edu.cn; wtq@tsinghua.edu.cn; chengjie11@tsinghua.org.cn; liuyuhong@tsinghua.edu.cn; xclu@tsinghua.edu.cn).

Y. Peng is with the Department of Computer Science and Computer Engineering, University of Arkansas, Fayetteville, AR 72701 USA (e-mail: yrpeng@uark.edu).

S. K. Lim is with the School of ECE, Georgia Institute of Technology, Atlanta, GA 30318 USA (e-mail: limsk@ece.gatech.edu).

Color versions of one or more of the figures in this paper are available online at http://ieeexplore.ieee.org.

Digital Object Identifier 10.1109/TSM.2017.2688498

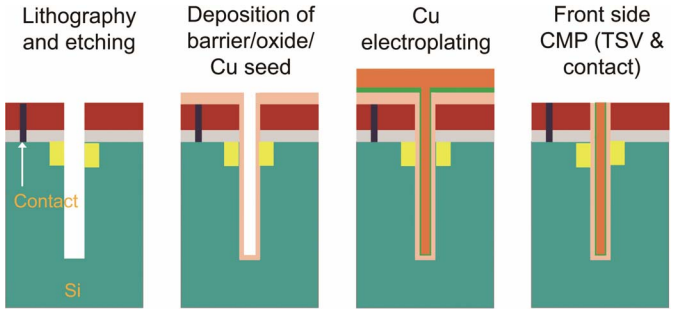

Fig. 1. Via-middle process schematic [7].

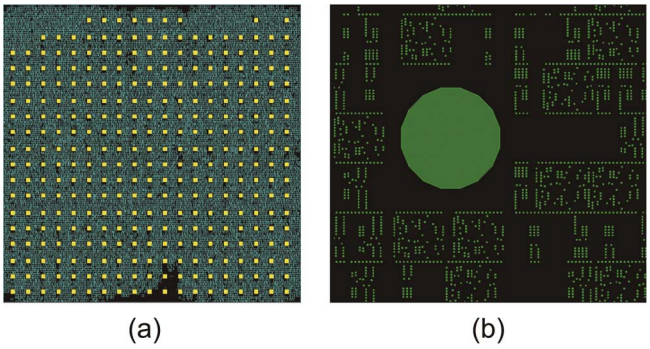

Fig. 2. TSVs and contacts in a full-chip 3D IC (top die shown). (a) Die placement with 330 TSVs, (b) Single TSV and its neighboring contacts.

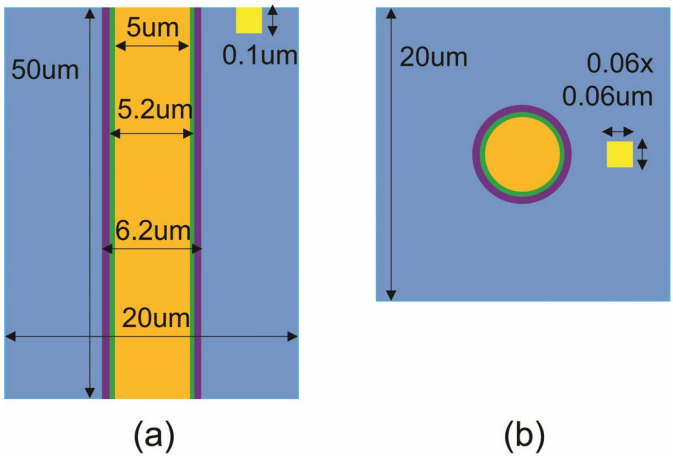

Fig. 3. Model structure with TSV and contact. (a) Cross sectional view, (b) Top view.

After creating the device on a wafer front side in the via-middle process, we created interconnect wires, including the Metal 1 or Metal 2 layer, before making the TSV. Because of its small size, the contact could easily be over polished, thus revealing and even damaging the device. Therefore, we must strictly control the CMP removal's thickness. Adding a stop layer, such as a silicon nitride layer, or tuning the slurry selectivity by adding oxidant and corrosion inhibitors are the most commonly used methods for slowing down the material removal rate. The TSV annealing process is also a breakthrough point to optimize the CMP results and profile. In some cases, steps will be taken as follows: CMP step, annealing, and another CMP step to help reduce the stress and pop-out problems induced by annealing. Therefore, if we can obtain or accurately predict the TSV and contact pop-out height after annealing and control the initial CMP dishing to balance it to a certain degree, then we do not have to perform the second CMP step. This will prevent the accumulation of defects induced by CMP and reduce the manufacturing cost.

In this study, we focused on the post-annealing stress and pop-out results of TSVs and contacts in the via-middle process. We demonstrated that the TSV-to-contact distance has little impact on the TSV, while it has a significant impact on contact. This is mainly due to the large size difference between the TSV and the contact. Then we showed that material plasticity is of great importance to annealing results and that plastic deformation must be taken into consideration. We also demonstrated that all of the stress and pop-out results for TSVs and contacts increased as the annealing temperature increased. Therefore, a relatively low temperature is needed in practical fabrication. In addition, we proposed several types of models to see the effect of the nearest neighboring contacts on the center contact. Finally, we used the linear superposition method to predict the stress and verified its accuracy by comparing it with the finite element analysis (FEA) simulation. It was determined that it was an applicable and meaningful approach to forecast and tune the stress of full-chip design.

II. Simulation Methodologies

In this section, we will demonstrate our design and simulation methodologies for the TSV-contact model in detail. Our models were based on a 64-point fast Fourier transform (FFT64) design which is implemented on a 2-die 3D IC using 45 nm technology [23], [24]. The TSVs and contacts are shown in Fig. 2(a), and a single TSV and its neighboring contacts are shown in Fig. 2(b).

A. Library Construction

We created 3D FEA models for the TSV and contact structure using the commercial simulation tool, ABAQUS [21]. We constructed two models: single TSV, single contact and single TSV, multiple contact. The model structure comprised five parts: Cu TSV, diffusion barrier, oxide liner, W contact, and Si substrate. Fig. 3(a) and Fig. 3(b) present the cross section and top view of the structure, respectively. The baseline TSV diameter, height, diffusion barrier thickness, oxide liner thickness, side contact length, and contact height are 5μm, 50μm, 0.1μm, 0.5μm, 0.06μm, and 0.1μm, respectively. We used Ti and SiO_2 as the diffusion barrier and oxide liner, respectively. Table I gives the annealing process used in the simulation: heating from 25°C to a certain temperature for 20 min, maintaining this temperature for 20 min, then cooling down back to 25°C for 50 min. We only carry out simulations for low temperature annealing ($<$ 400 °C) in order to avoid re-crystallization and diffusion [25].

B. Simulation Settings

We chose the following simulation settings carefully, and Table II presents the simulation results for the TSV and contact.

TABLE I
MATERIAL PROPERTIES

Material	CTE (ppm/K)	Young's modulus (GPa)	Poisson's ratio
Cu	17	110	0.35
SiO2	0.5	71	0.16
Si	2.3	130	0.28
W	4.5	411	0.28
Ti	8.6	116	0.32

TABLE II
COMPARISON OF TSV RESULTS WITH DIFFERENT SETTINGS. THE MODEL SIZE IS FIXED AT 50 μM × 50 μM × 125 μM.√ MEANS DEFAULT VALUE

Settings	Options	Heat stress (MPa)	Cool stress (MPa)	Heat height (nm)	Cool height (nm)
Unit	Basic	883	240	485	131
	Micrometer√	907	250	485	129
Mesh size	2.5 μm√	1033	357	569	114
	2 μm	1036	355	569	114
	1.8 μm	1034	352	569	113
Fixed boundary	One side	2965	1194	94	8.15
	Five sides√	5704	1145	43	8.03
TSV sidewall angle	90°√	1033	357	569	114
	88°	975	334	561	113.5

Unit System: The minimum value accepted by ABAQUS is 10^{-5}, but the smallest size in our model is a 0.06 μm contact size. Therefore, it is difficult to use the standard unit system. We converted the standard unit system into a system that uses μm as the length unit and called it the micrometer unit system. Table II lists the TSV results in different settings. In the standard unit system, there is only TSV and no contact. The two unit systems have very similar results, which demonstrate that our micrometer unit system conversion is correct. Therefore, we performed the following simulations based on this micrometer unit system.

Mesh Size: We studied whether the mesh size and quantity would have an impact on the stress and pop-out. We performed three simulations by changing the mesh size, the number of the main parts in the model, and the Si substrate. As shown in Table II, the TSV stress and pop-out height barely change as the mesh size changes. This shows that the impact of the meshing method is very small. To decrease the number of meshes, we chose 2.5 μm as the main mesh size, which is the mesh size of Si substrate. In addition, we used mesh sizes of 0.01 μm for the contact, 1 μm for the TSV, and 0.5 μm for the barrier and oxide liner.

Boundary Conditions: We used two types of boundary conditions. One was used to fix the bottom face of the TSV in place to prevent displacement and rotation, and the other was used to fix all five faces except the top face. The results showed that the TSV stress and pop-out after heating were largely affected when the fixed boundary changed from one to five faces. Stress accumulated because the TSV tended to expand, but the four sidewalls restricted its expansion. The pop-out after heating decreased because the sidewalls are fixed, and the Si substrate exhibited a small displacement, thus pulling the TSV. The results after cooling show minor changes. In an actual structure, thermal expansion is restricted by sidewalls; hence, the condition is much closer to a five-faces-fixed boundary condition, which was applied in our simulations.

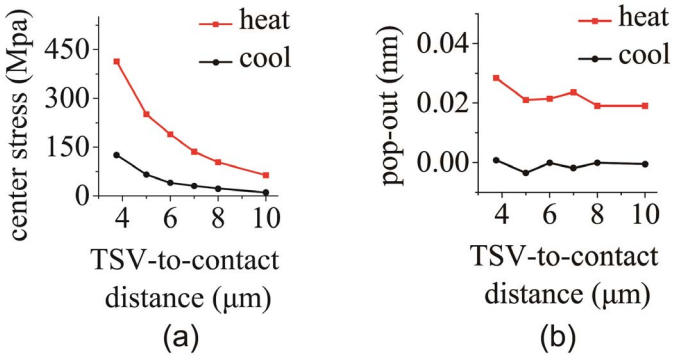

Fig. 4. Contact center stress and pop-out height in different TSV-to-contact distances. (a) Von Mises stress, (b) Pop-out height after heating and cooling.

TSV sidewall angle: we applied two angles in the simulation. One is 90° and the TSV model is a cylinder, the other is 88° [26] and the TSV is a circular cone. We compare the two models and see the impact of sidewall angle on the analysis result. As Table II shows, When the TSV sidewall angle changes from 90° to 88°, the TSV stress after heating decreases by 5.61% and by 6.44% after cooling, while the TSV pop-out height decreases by 1.41% and 0.44% after heating and cooling, respectively. This illustrates that the form factor of TSV and the sidewall angle show noticeable impacts on analysis results. The TSV stress and pop-out height decrease when the TSV model is a circular cone. Since the difference between 90° and 88° is small, and the annealing process is less sensitive to the sidewall angle, we assume TSVs as cylinders in the following part of this paper.

III. TSV-TO-CONTACT DISTANCE IMPACT

In this section, we describe several simulations employed to study the impact of TSV-to-contact distance on the stress and the pop-out height. The simulation runtime was approximately 5-6 h for the single TSV, single contact model, and 33 h for the single TSV, 34 (multiple) contact model.

A. Single TSV, Single Contact Model

1) Impact on Stress and Pop-Out Height: As the dimensions of a TSV are very large compared to the dimensions of a contact, the distance between the two has very little impact on the potential size of a TSV. The difference is small even between a model that contains only a TSV and a model that contains a TSV and a contact. However, the distance between the two has a large influence on contact results. Fig. 4 shows the center stress and pop-out height of the contact at different TSV-to-contact distances. At a certain point, the stress is a tensor that has several components in different directions. To simplify the results, we only focused on the Von Mises stress. As the distance between the TSV and the contact increased, the center stress of the contact decreased after both heating

TABLE III
DETAILED COMPARISON OF DIFFERENT TSV-TO-CONTACT DISTANCES

Type	d4 heat stress (MPa)	d8	d4 cool stress (MPa)	d8	d4 heat height (nm)	d8	d4 cool height (nm)	d8
TSV	165	↓	217	↓	91	↑	5.08	↓
contact	397	↓↓	115	↓↓↓	0.025	↓↓	-0.002	↓↓↓

and cooling. This is due to a reduction in the impact of TSV expansion or reduction on the contact. The stress after heating was always larger than that after cooling. This is because the materials are in the elastic region, and the Cu TSV will expand intensively in the heating process and push on to the surrounding Si. The CTE of Cu is much larger than Si; therefore, a large amount of stress accumulates on the nearby Cu contacts. However, most of the material deformation is elastic deformation, so the TSV and Si contracted during the cooling process. This behavior complies with the expected behavior of these materials and relieves the stress. For contact pop-out, as the distance between the TSV and the contact increased, after heating the pop-out decreased by a small amount, and after cooling it decreased by even less. Because the contact structure is too small and is only on the top surface of the Si substrate, its deformation is also small; the TSV only has a limited impact. The pop-out after heating is larger than the pop-out after cooling because of the expansion and reduction of the contact during heating and cooling, respectively. Pop-out may have a negative value after cooling because the CTE of W is larger than Si, in a condition known as dishing. Therefore, the contact will expand to a greater extent than Si when heated and contract to a greater extent when cooled. This behavior explains why the contact pop-out has both positive and negative values after the cooling process.

2) TSV-to-Contact Distance Comparison (4 μm vs. 8 μm): We compared 4 μm (d4) and 8 μm (d8) TSV-to-contact distances to further investigate this issue. Table III shows the results. The up arrow means that the result in d8 increased compared to d4, and the down arrow means that the result in d8 decreased compared to d4. The number of arrows represents the degree of change. For the TSV, there is only approximately a 2% change in stress or pop-out because the contacts are too small. The stress in the TSV during heating and cooling decreased slightly when the distance was changed from d4 to d8 because the impact of the contact on the TSV was smaller at d4. The pop-out at d8 increased slightly after heating and decreased slightly after cooling because the TSV was easier to deform when expanding and contracting. However, the impact of TSV-to-contact distance was much larger on the contacts than it was on the TSV. More than 30% of stress change and more than 60% of pop-out change were observed on the contacts nearby because TSV pushes or pulls the contacts much more intensively. In d8, the impact of TSV push or pull on the contact was smaller than in d4, so both the contact stress and pop-out height dropped after heating and cooling.

B. Single TSV, Multiple Contact Model

The TSV-to-contact distance also has an impact on the single TSV, multi-contact model. We performed simulations for a model with 1 TSV and 34 contacts. For this FFT circuit, since we originally set the keep-out zone (KOZ) as 0.5 μm [23], the minimum TSV-to-contact distance is calculated by adding up TSV radius (2.5 μm), barrier thickness (0.1 μm), oxide liner thickness (0.5 μm), KOZ (0.5 μm), and half of the contact length (0.03 μm), which is 3.63 μm in total. Therefore, the TSV-to-contact distance has the constraint of minimum distance, which is 3.63 μm. We chose three contacts at different distances of 5.29 μm, 3.67 μm, and 3.63 μm. The results are given in Fig. 5 and Table IV. When the TSV-to-contact distance changes from 5.29μm to 3.67μm and 3.63μm, the contact center stress after heating increases. The difference is 20.6% from 5.29μm to 3.67μm, and 1.76% from 3.67μm to 3.63μm. This also applies to the contact center stress after cooling, which increases 1.27X from 5.29μm to 3.67μm, and 2.94% from 3.67μm to 3.63μm. As for the pop-out height in contact center, it has a small oscillation. The pop-out after heating decreases by 8.8% when the TSV and contact gets closer from 5.29μm to 3.67μm, but the pop-out after cooling increases by 37.5%. When the distance decreases from 3.67μm to 3.63μm, the pop-out height after heating stays the same and the cooling height increases a little by 9.1%. Therefore, the impact of TSV-to-contact distance in single TSV multiple contact model shows the same trend as the single TSV single contact model.

TABLE IV
CONTACT CENTER STRESS AND POP-OUT HEIGHT AT DIFFERENT DISTANCES

TSV-to-contact distance	Heat stress (MPa)	Cool stress (MPa)	Heat height (nm)	Cool height (nm)
5.29	330	105	0.034	-0.008
3.67	398	238	0.031	-0.011
3.63	405	245	0.031	-0.012

IV. MATERIAL PLASTICITY IMPACT

In this section, we discuss simulations conducted to gain an understanding of the impact of material plasticity. In some simulation studies, the material was set to have only elastic deformation but not plastic deformation. These results may not provide a satisfactory level of accuracy. We performed simulations for different plasticity parameters, discussed the impact, and demonstrated that material plasticity and plastic deformation are of vital importance to the result.

The elastic limit of Cu is 80 MPa and the offset yield strength is 142 MPa. The elastic limit of W is 310 MPa, and the offset yield strength is 515 MPa. When the stress is below the elastic limit, we define this as the elastic region. When the stress is slightly above the elastic limit, we define the region

TABLE V
PLASTICITY IMPACT: SINGLE TSV, SINGLE CONTACT MODEL; DEFAULT PLASTICITY

Region	Anneal temp. (°C)	TSV-to-contact dist. (μm)	Plastic	Heat stress (MPa)	Cool stress (MPa)	Heat height (nm)	Cool height (nm)
			TSV				
elastic	175	4	default	119	78	52	1.21
plastic	375	4	default	196	229	143	21
			Contact				
elastic	175	8	default	204	129	0.029	-0.007
plastic	375	8	default	236	412	0.28	-0.24

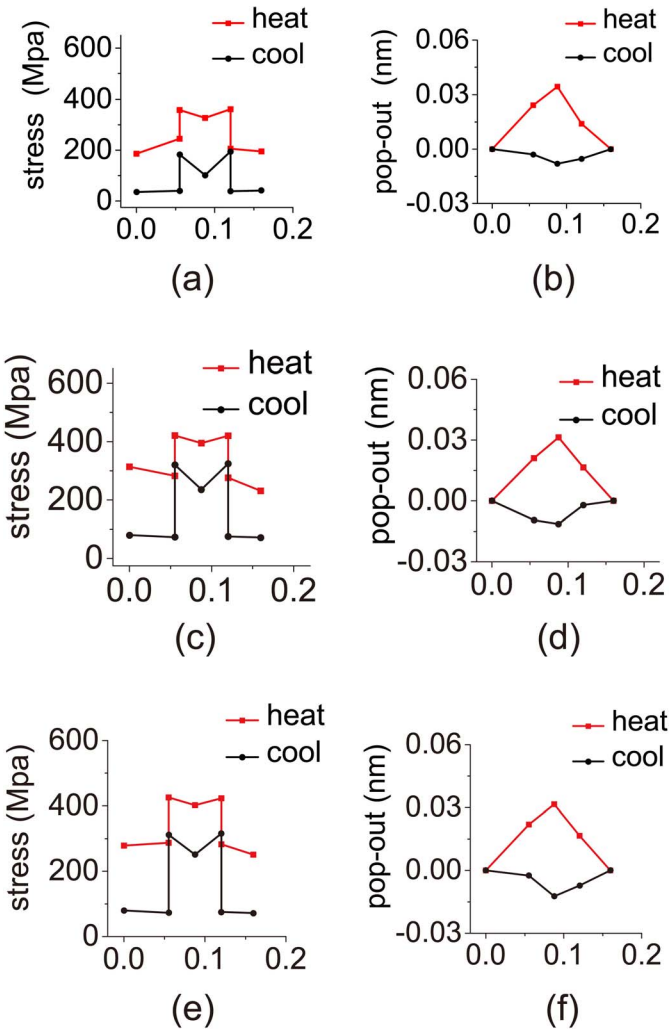

Fig. 5. Contact results along a path in the multi-contact model. The x-axis represents the distance along the path that passes through the contact. The TSV-to-contact distance is 5.29 μm in (a) and (b), 3.67 μm in (c) and (d), and 3.63 μm in (e) and (f).

as the elastic-dominated region because elastic deformation is still the dominant behavior. When the stress is near or over the offset yield strength, we define the region as the plastic-dominated region. When the material plasticity increases, the stress needed for the same strain decreases. For a TSV, we focused on the impact of Cu plasticity on the TSV. For the contact, we focused on the impact of W plasticity. The simulation runtime was approximately 5-6 h for the single TSV, single contact model and 8 h for the single TSV, 8 contact model.

TABLE VI
PLASTICITY IMPACT: SINGLE TSV, SINGLE CONTACT MODEL; ELASTIC-DOMINANT REGION

Region	Anneal temp. (°C)	Plastic strain	Heat stress (MPa)	Cool stress (MPa)	Heat height (nm)	Cool height (nm)
			TSV			
elastic	175	0.5 Cu	130	69	52	0.98
	175	Cu	119	78	52	1.21
	175	2 Cu	110	89	53	1.77
			Contact			
elastic	275	0.5W	406	111	0.029	-0.006
	275	W	394	140	0.031	-0.008
	275	2 W	381	167	0.034	-0.011

A. Single TSV, Single Contact Model

1) Elastic vs. Plastic Regions: Table V shows the plasticity impact results in different material regions. In the TSV elastic-dominated region, the TSV stress after cooling was 34.5% lower than that after heating, and the pop-out after cooling was very small: approximately 2.3% of the height after heating. This is because most of the TSV deformation was elastic. When the thermal load was released, the expanded area contracted. However, in the plastic-dominated region, the TSV stress after cooling was 16.8% larger than the stress after heating, and the pop-out after cooling was larger than that in elastic-dominated region: approximately 17.4 times larger. This is because most of the TSV expansion goes through plastic deformation, and therefore cannot contract. The trend for the contact result is similar to the TSV results.

2) Plasticity Impact in the Elastic-Dominated Region: Table VI, Fig. 6, and Fig. 7 present the plasticity impact results and curves along a path with different Cu or W plasticity in the elastic-dominated region. For the TSV, as Cu plasticity increased by a factor of three, the stress after heating decreased and had a total drop off of 15.4%. This is because only a smaller stress is needed to obtain the same strain. The stress after cooling increased by 29% because it was the remaining deformation that dominated, so a larger pop-out led to a larger stress. The TSV stress after cooling was lower than that after heating because of the contraction. The pop-out increased by 1.9% and 80.6% after heating and cooling, respectively because Cu became easier to deform and maintained its deformation when the plasticity increased.

The contact results follow the same trend as the TSV results. The contact stress after heating decreased by 6.6%, and the stress after cooling increased by 50.5% when the W plasticity

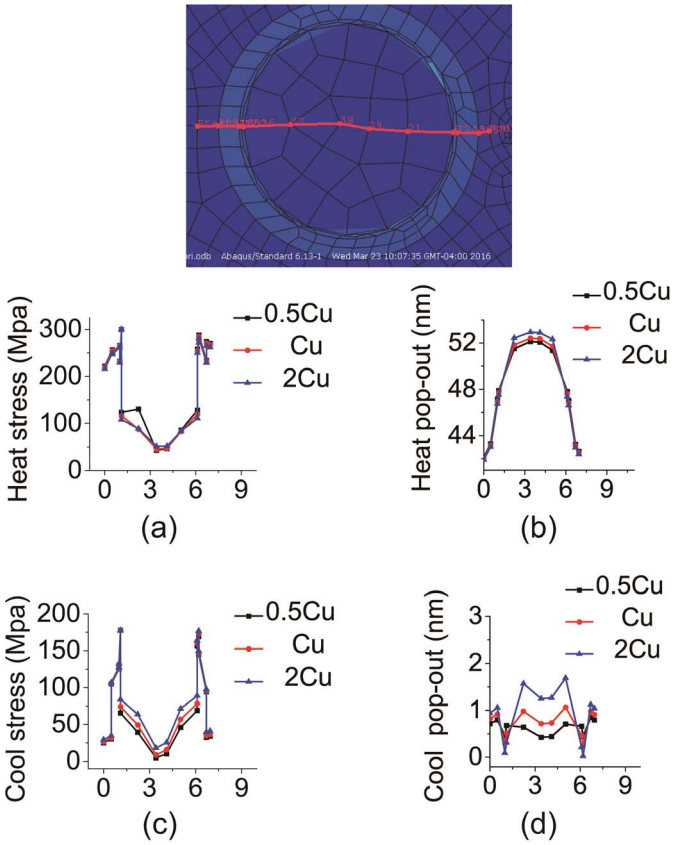

Fig. 6. TSV results for different Cu plasticity; elastic-dominant region. The x-axis represents the distance along the path that passes through the TSV.

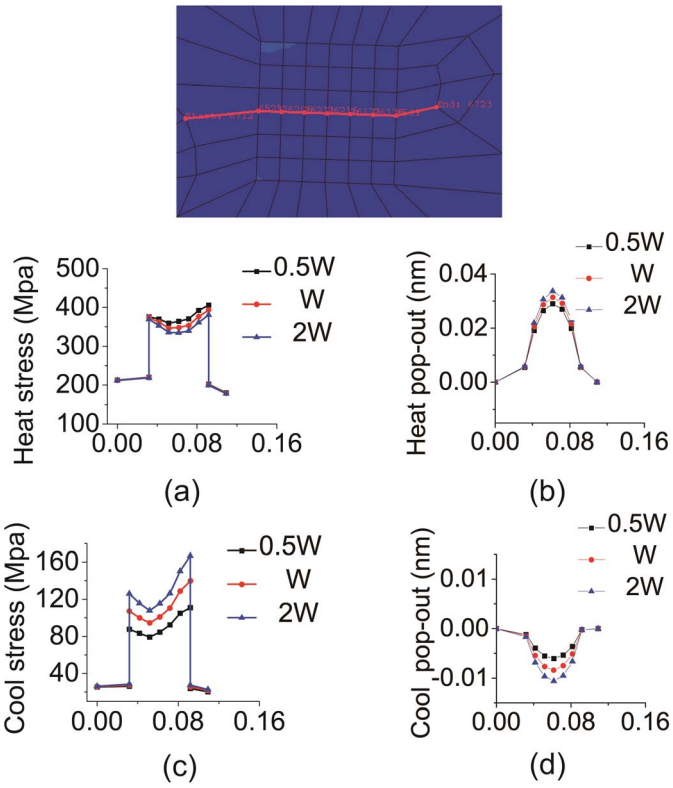

Fig. 7. Contact results for different W elasticity; elastic-dominant region. The x-axis represents the distance along the path that passes through the contact.

increased by a factor of three. The pop-out increased by 17.2% after heating and by 83.3% after cooling.

3) Plasticity Impact in the Plastic-Dominated Region: Table VII shows the plasticity impact results in the plastic-dominated region. As the Cu plasticity increased by a factor of three, the TSV stress experienced a decrease of 6.8% and 8.8% after heating and cooling, respectively. This is because only a smaller stress is needed obtain the same strain and deformation. The stress after cooling is higher than after heating, because stress accumulates even in the cooling phase. The pop-out increased by 6.5% and 22.7% after heating and cooling, respectively.

For the W contact, the trend is the same as with the TSV. The contact stress experienced a drop of 17.2% and 18.8% as the W plasticity increased from a factor of 0.5 to a factor of two. The pop-out increased by 15% and 31.4% after heating and cooling, respectively.

TABLE VII
PLASTICITY IMPACT: SINGLE TSV, SINGLE CONTACT MODEL; PLASTIC-DOMINANT REGION

Region	Anneal temp. (°C)	Plastic strain	Heat stress (MPa)	Cool stress (MPa)	Heat height (nm)	Cool height (nm)
			TSV			
plastic	375	0.5 Cu	205	239	139	22
	375	Cu	196	229	143	21
	375	2 Cu	191	218	148	27
			contact			
elastic	375	0.5W	563	626	0.060	-0.035
	375	W	520	559	0.064	-0.040
	375	2 W	466	508	0.069	-0.046

B. Single TSV, Multiple Contact Model

For the single TSV, multiple contact model, the rules are the same as with the single, TSV, single contact model. Considering a Cu TSV, as Table VIII shows, Cu is in the plastic-dominated region and the trend is the same as with the single contact case. As the Cu plasticity increased, the TSV stress decreased to 65% and 88% of default after heating and cooling. The pop-out increased by 2.2% and 37.7% after heating and cooling. For the contact, the stress of W is very close to plastic-dominated region, so the trend is close to plastic-dominated case. As the W plasticity doubled, the contact stress experienced a decrease of 12.5% and 0.96% after heating and cooling, respectively. The pop-out increased by 16.7% after cooling.

V. ANNEALING TEMPERATURE IMPACT

In this section, we demonstrate the impact of annealing temperature on TSVs and contacts, as shown in Table IX. It is obvious that when the temperature increases, the TSV stress and the pop-out height, as well as the contact stress and the pop-out deformation, all increase after heating and cooling. When the annealing temperature increased from 275 °C to 375 °C, the stress level of the TSV increased by 18.8%, and the pop-out height increased by a factor of 3.13.

TABLE VIII
PLASTICITY IMPACT: SINGLE TSV, MULTIPLE CONTACT MODEL; PLASTIC-DOMINANT REGION

Anneal temp. (°C)	Plasticity	Heat stress (MPa)	Cool stress (MPa)	Heat height (nm)	Cool height (nm)
		TSV			
275	Default	220	469	90	5.3
	2 Cu	143	413	92	7.3
		Contact			
275	Default	448	416	0.077	-0.006
	2 W	392	412	0.077	-0.007

TABLE IX
ANNEALING TEMPERATURE IMPACT

Anneal temp. (°C)	Type	Heat stress (MPa)	Cool stress (MPa)	Heat height (nm)	Cool height (nm)
		Single TSV, single contact			
275	TSV	165	217	91	5.08
375	TSV	196	229	143	21
275	Contact	497	482	0.042	-0.020
375	Contact	520	559	0.064	-0.040
		Single TSV, multi-contacts			
275	TSV	220	469	90	5.34
375	TSV	323	572	140	21
275	Contact	448	416	0.077	-0.006
375	Contact	531	531	0.087	0.023

At the same time, the stress level for the contacts increased by 15.9%, and the pop-out height increased by 100%. This trend was expected because when the temperature is high, material expansion during heating and contraction during cooling are intensive for Cu and W. Therefore, the stress increased and the deformation grew.

According to the results for the single TSV, multiple contact model, the trend is the same as that seen in the single TSV, single contact model. The stress and the pop-out height increased after heating and cooling. When the temperature increased by 100 °C, the stress and the pop-out for the TSV increased by a maximum of 46.8% and by a factor of 2.93, respectively. At the same time, the stress and pop-out for the contact increased by a maximum of 27.6% and by a factor of 2.83 for the contact.

VI. NEAREST NEIGHBORING CONTACTS

In this section, we discuss the impact of neighboring contacts and showed that the distribution of the contacts has a significant impact on the stress and the pop-out height. Table X compares the center contact results with or without the nearest neighboring contacts. When there were nearest neighboring contacts, the center contact showed a stress increase of 12% after heating and 37% after cooling. This is because the expansion or contraction of the center contact was restricted by the nearest neighboring contacts. In addition, the pop-out increased by 0.081 nm after heating and by 0.008 nm after cooling because of the presence of the nearest neighboring contacts. They impose limitations on the center contact, which leads to increased deformation.

TABLE X
NEIGHBORING CONTACT IMPACT, TSV-TO-CONTACT DISTANCE IS 4 um

Contact number	Neighbor ?	Center to neighbor contact dist. (μm)	Heat stress (MPa)	Cool stress (MPa)	Heat height (nm)	Cool height (nm)
8	No		347	237	0.032	0.011
12	Yes	0.5	389	325	0.113	0.019
12	Yes	0.3	364	364	0.150	0.026

When the distance of the nearest neighboring contact changes, the impact on the center contact also changes. When the distance between nearest neighboring contacts and the center contact decreased from 0.5 μm to 0.3 μm, the center contact stress increased by 12.6% and 12% after heating and cooling; the pop-out height increased by 32.7% and 36.8%, respectively. This was because the restriction imposed on the center contact owing to the presence of the neighboring contacts.

In summary, the overall post-annealing TSV stress was approximately 300-400 MPa, and the pop-out ranged from 5-21 nm in our simulation. According to the study by Moogon *et al*. [12], the post-annealing stress should be around 250-600 MPa. On the other hand, in the study conducted by Saettler *et al.* [14], Ji *et al.* [15], and He *et al.* [16], the post-annealing pop-out should range from 30 nm to 300 nm. Typically, we observe an average dishing of 20-30 nm in a TSV CMP process. Therefore, it is feasible to control the post-annealing pop-out and post-CMP dishing by carefully tuning these key parameters.

VII. LINEAR SUPERPOSITION METHOD

For complicated structures that incorporate hundreds of TSVs and millions of contacts, FEA simulation requires too much time and effort. However, the principle of superposition can be effective in this type of application. The linear superposition method states that the effect that a number of simultaneously-acting forces have on a body can be calculated by adding the sum of the effects of the forces when applied separately. This method can be applied to the determination of stress and displacement. Therefore, we used this method to add all of the individual stress tensors at a point to compute the stress. The total stress included the stress caused by each TSV and the stress caused by each contact.

We demonstrated the simulation by varying the number of TSVs and contacts. We obtained the stress results for simple models from simulation and superposition; we then validated the accuracy of the superposition by comparing the results. Then, we performed a simulation for complicated models and predicted the result (this is very meaningful for full-chip prediction). We set the minimum TSV pitch to 10 μm. For stress caused by a TSV, we used FEA simulations to obtain the stress tensors along a radial line from the TSV center in a single TSV structure. For stress caused by a contact, we obtained the stress tensors from the contact center in a single contact structure. In the following linear superposition method, we divided the simulation area into a non-uniform array style grid with a 0.1

TABLE XI
VON MISES STRESS COMPARISON BETWEEN FEA SIMULATIONS AND THE LINEAR SUPERPOSITION METHOD

# TSV	# contact	FEA simulation		Linear superposition method	
		# node	Run time	# sim point	Run time
1	1	28K	6.5 h	0.25M	3.9 s
				25M	687 s
1	10	309K	18.5 h	0.25M	15.5 s
				25M	2,928 s
2	10	465K	28.5 h	0.25M	26.7 s
				25M	4,334 s
5	144	450K	36 h	0.66M	1,200 s
				6.25M	20,700 s
9	256			0.74M	1,911 s
				6.25M	28, 576 s

μm pitch in TSV areas and a 0.01 μm pitch in contact areas. If the stress tensor at a grid point could not be obtained directly from the stress tensor list, we used linear interpolation with adjacent stress tensors from the list to compute the stress. In addition, we used the stress in the contact center to represent the entire contact area in the superposition method, as there are too many contacts in the full-chip design, and each contact is too small.

Table XI shows some of our comparisons. We could see that there was a huge reduction in run time with the linear superposition method. Although the linear superposition method performs the stress analysis on a two-dimensional (2D) plane, we could perform the analysis on other planes in a similar way if needed. In addition, the run time shows dependency on the number of simulation points, which is related to the number of TSVs and contacts. This demonstrates that the linear superposition method is scalable and can be applied to full-chip analysis.

A. Simulation and Superposition for 1 TSV 10 Contacts Model

Fig. 8 shows the von Mises stress map for the single TSV 10 contacts model case. The distance from contact 5/contact 10 to TSV is 3.75 um, and the color scale is the same. It is clear that the linear superposition method matches very well with the FEA simulation results. The stress distribution matches in the TSV area. As we used the center stress to cover the entire area for the contact, we compared the stress data in contact center of both the FEA simulation and the linear superposition method. Fig. 9 shows the data comparison for contact stress. We can see that the results of the superposition and the FEA simulation were close; the minimum deviation is 8%. The results in the FEA simulation were not exactly symmetrical; this is because the meshing in the FEA software is not very symmetrical.

B. Simulation and Superposition for 2 TSV 10 Contacts Model

We increased the number of TSVs to two, and studied the comparison between the simulation and superposition methods in the next analysis. The TSV-to-TSV distance was set at

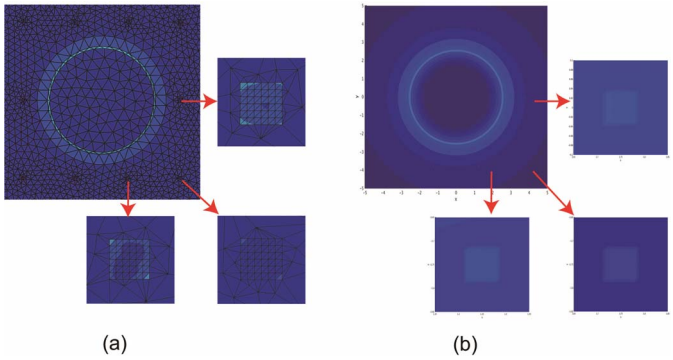

Fig. 8. Stress map comparison of von Mises stress between FEA simulation and the linear superposition method. (a) FEA simulation result, (b) Superposition result.

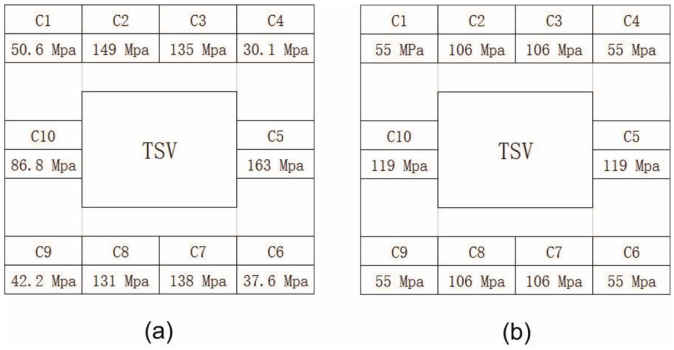

Fig. 9. Contact stress data comparison of von Mises stress between FEA simulation and the linear superposition method. (a) FEA simulation result, (b) Superposition result. Stress values are in MPa.

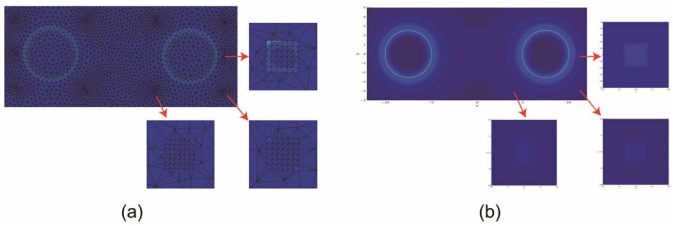

Fig. 10. Von Mises stress map comparison between the FEA simulation and the linear superposition method. (a) FEA simulation result, (b) Superposition result.

15 um, and the distance of contact 5/contact 10 to the nearest TSV as 3.75 um. Fig. 10 and Fig. 11 present the stress maps and contact stress data of the FEA simulation and the linear superposition method. The data shows that the superposition results were very close to the FEA simulation. The minimum deviation between the two datasets was 4.9%.

C. Simulation and Superposition for 5 TSV 144 Contacts Model

The comparison for a 5 TSV 144 contacts model is given in Fig. 12 and Fig. 13. In this comparison, the contact center stress is symmetrical in superposition and nearly symmetrical in the FEA simulation. The minimum deviation between the two datasets was 7.4%. In general, the superposition results were close to FEA simulation, and were obtained in far less time.

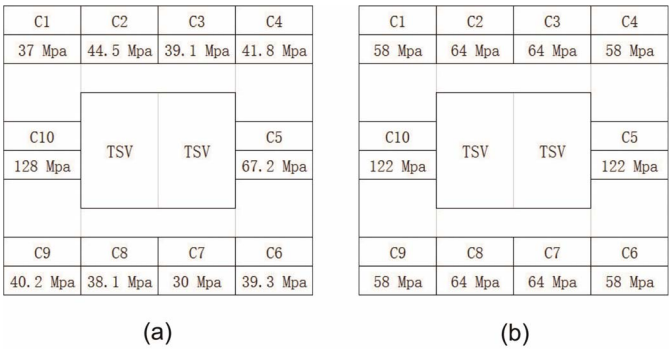

Fig. 11. Von Mises stress data comparison between the FEA simulation and the linear superposition method. (a) FEA simulation result, (b) Superposition result. Stress values are in MPa.

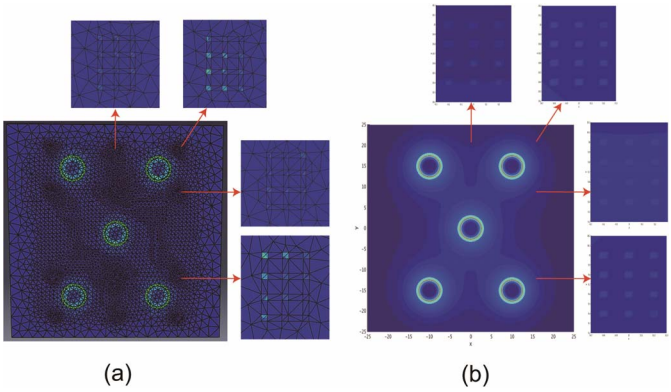

Fig. 12. Von Mises stress map comparison between the FEA simulation and the linear superposition method. (a) FEA simulation result, (b) Superposition result.

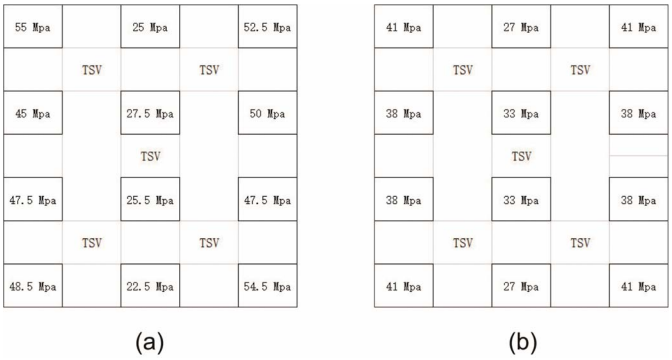

Fig. 13. Von Mises stress data comparison between the FEA simulation and the linear superposition method. (a) FEA simulation result, (b) Superposition result. Stress values are in MPa.

D. Superposition for Complicated Models

Finally, we predict the stress for more complicated models because the FEA simulation takes too much time. We establish a model with 9 TSVs and 256 contacts, and conduct the FEA simulation and linear superposition method again. Fig. 14 shows the stress distribution map of TSVs and contacts, as well as a three-dimensional view. Fig. 15 shows the contact center stress of 12 different groups; for each group we choose the contact in the same location. These obtained results are reasonable and match the expected data.

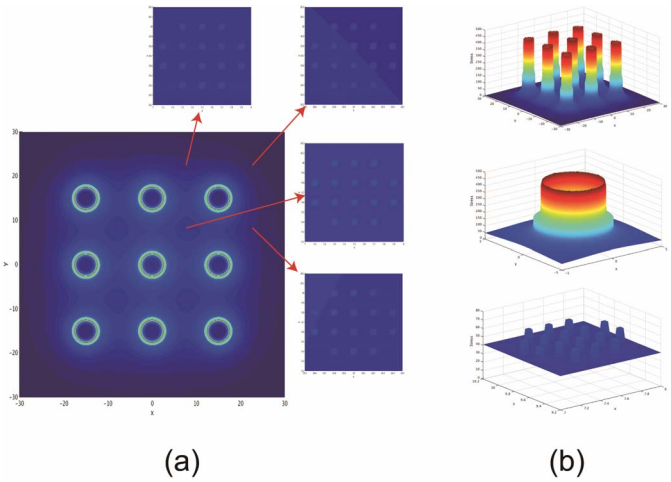

Fig. 14. Von Mises stress map using the linear superposition method, the model contains 9 TSVs and 256 contacts. Stress values are in MPa.

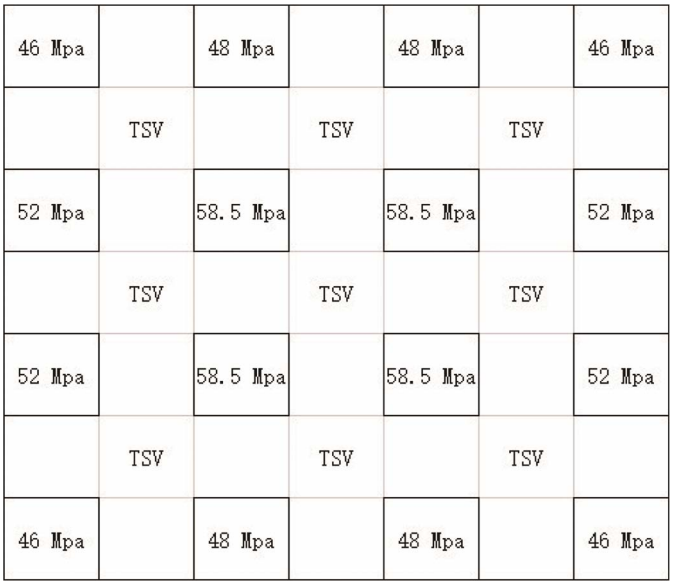

Fig. 15. Von Mises stress contact center stress data using the linear superposition method, the model contains 9 TSVs and 256 contacts.

Furthermore, we demonstrated linear superposition method for a model containing100 TSVs and 9801 contacts, the model is in regular design. Fig. 16 shows the stress distribution map for TSVs and contacts. This proves that the linear superposition method is capable of predicting the stress for a model with many TSVs and contacts, and therefore it can be used to perform a full-chip analysis.

In summary, the linear superposition method could greatly reduce run time for stress analysis, while maintaining a high level of accuracy. It offers the best approach to obtain the stress distribution for a full-chip design.

VIII. CMP Cost Model

Our ultimate goal is to tune and optimize the CMP process by predicting the post-annealing stress and pop-out. CMP performance is characterized by many parameters, including material removal rate, non-uniformity, etc. [27]. In this

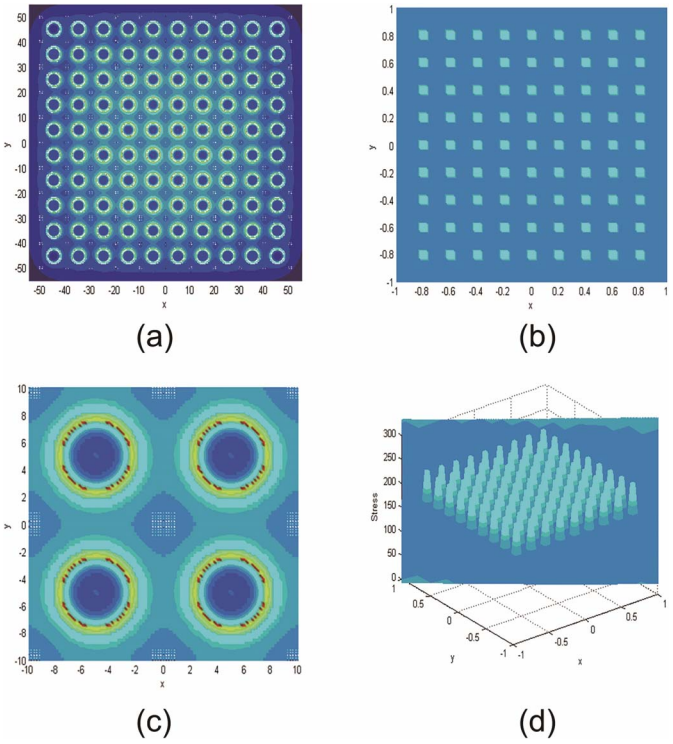

Fig. 16. Von Mises stress map in linear superposition method, the model contains 100 TSVs and 9801 contacts. (a) General stress map, (b) stress map for contacts, (c) stress map for TSVs, (d) 3D stress map for contacts.

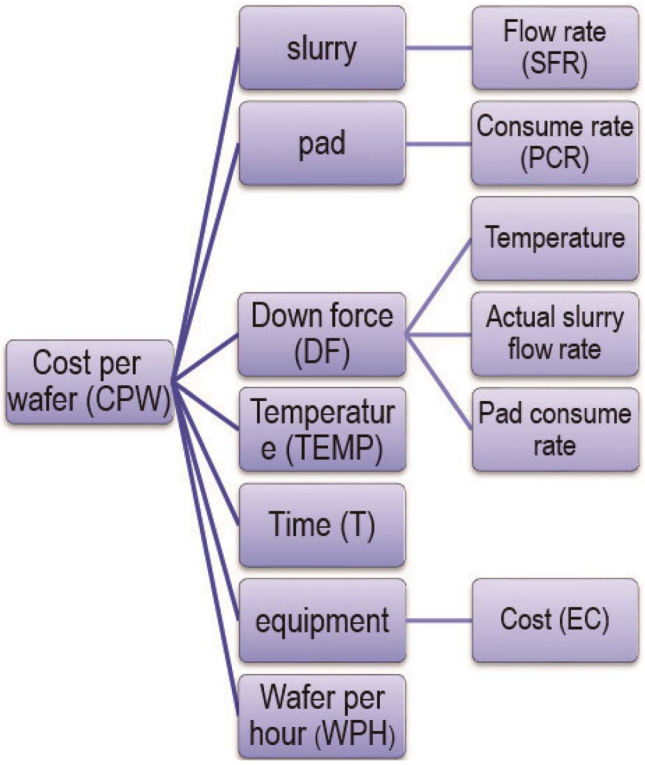

Fig. 17. Parameters for consideration in the CMP cost model.

work we focus on reducing the CMP cost. A co-optimization of the CMP parameters and post-annealing stress/pop-out is significant to provide overall guidelines. First we propose a CMP cost estimation model with every technology parameter included to link the stress and pop-out to CMP cost. Then we took many parameters into consideration, including CMP slurry, pad consumption, polishing down force, wafer per hour (WPH) capacity, etc. Assuming that the model was linear with WPH as the denominator, we gave a range for the weight of parameters, and obtained the relationship between input and output. Finally, we were able to obtain an output range for any input range.

Fig. 17 shows the parameters for the CMP cost model. The input parameters were: slurry flow rate (SFR), down force (DF), and equipment cost (EC, assume it is a constant). The output parameters were wafer per hour (WPH), pad consumption rate (PCR), temperature (TEMP), and time (T). ΔCPW, ΔPCR, and ΔDF were the parameters calculated. The post-annealing stress and pop-out have a relationship with CMP parameters, particularly with the input parameters such as ΔSFR and ΔDF, and we connected these to CMP cost. Table XII lists the CMP cost summary for these parameters. Except for the change in polishing down force, the cost of which decreases when down force increases, other terms were all positive for CMP cost. This means that increasing slurry flow rate, as well as post-annealing stress/pop-out, will have an increasing effect on CMP cost. Therefore, we should reduce post-annealing stress and pop-out in order to balance the related CMP cost.

TABLE XII
CMP COST MODEL SUMMARY FOR CHANGES OF DIFFERENT PARAMETERS

Fixed parameter	Changing parameter	Input range	Cost range
ΔDF	ΔSFR	10% - 20%	1.36% - 2.7%
ΔSFR	ΔDF	10% - 20%	-2.04% - -3.96%
ΔStress	ΔPop	10% - 20%	0.76% - 1.5%
ΔPop	ΔStress	10% - 20%	0.87% - 1.77%

IX. CONCLUSION

In this study, we investigated the post-annealing residual stress and pop-out of TSVs and contacts in via-middle processing. We demonstrated that the TSV-to-contact distance, material plasticity, annealing temperature, and nearest neighboring contacts have variable impacts on the residual stress of the TSV. We proved that when the TSV-to-contact distance changes, significant changes were observed on the contacts, while the TSV result experiences only a small change. To decrease the stress and pop-out, we should set a relatively larger distance between the TSV and the contact in industrial manufacturing. In addition, material plasticity has a large influence on stress and pop-out. Therefore, we took plasticity and plastic deformation into consideration during simulation. When the annealing temperature increased, the stress and pop-out results of the TSV and contacts increased significantly, so a lower annealing temperature is needed in fabrication as long as the circumstances permit. In addition, neighboring contacts also showed a significant impact on the center contact; therefore, all contacts should be arranged properly in

design and manufacturing. Finally, we conducted a comparison and validation between an FEA simulation and the linear superposition method. We demonstrated that the linear superposition method is a reliable and accurate approach to predict the post-annealing stress for full-chip design.

REFERENCES

[1] C. S. Selvanayagam *et al.*, "Nonlinear thermal stress/strain analyses of copper filled TSV (through silicon via) and their flip-chip microbumps," *IEEE Trans. Adv. Packag.*, vol. 32, no. 4, pp. 720–728, Nov. 2009.

[2] Y. Jiao *et al.*, "Tribological, thermal and kinetic attributes of 300 vs. 450 mm chemical mechanical planarization processes," *J. Electrochem. Soc.*, vol. 159, no. 3, pp. H255–H259, 2012.

[3] N. Habib *et al.*, "Deep trench capacitor in three dimensional through silicon via keepout area for electrostatic discharge protection," *IEEE Trans. Semicond. Manuf.*, vol. 29, no. 4, pp. 292–298, Nov. 2016.

[4] Z. Xu and J.-Q. Lu, "Through-silicon-via fabrication technologies, passives extraction, and electrical modeling for 3-D integration/packaging," *IEEE Trans. Semicond. Manuf.*, vol. 26, no. 1, pp. 23–34, Feb. 2013.

[5] T. C. Tsai *et al.*, "CMP process development for the via-middle 3D TSV applications at 28 nm technology node," *Microelectron. Eng.*, vol. 92, pp. 29–33, Apr. 2012.

[6] H. Philipsen *et al.*, "Metrology for monitoring and detecting process issues in a TSV module," *ECS J. Solid State Sci. Technol.*, vol. 3, no. 6, pp. Q109–Q119, 2014.

[7] M. Motoyoshi, "Through-silicon via (TSV)," *Proc. IEEE*, vol. 97, no. 1, pp. 43–48, Jan. 2009.

[8] V. S. Rao *et al.*, "TSV interposer fabrication for 3D IC packaging," in *Proc. 11th Electron. Packag. Technol. Conf.*, Singapore, 2009, pp. 431–437.

[9] P. C. Lin *et al.*, "TSV CMP process development and pitting defect reduction," in *Proc. Int. Conf. Planarization/CMP Technol. (ICPT)*, Grenoble, France, 2012, pp. 1–6.

[10] W.-H. Teh, D. Marx, D. Grant, and R. Dudley, "Backside infrared interferometric patterned wafer thickness sensing for through-silicon-via (TSV) etch metrology," *IEEE Trans. Semicond. Manuf.*, vol. 23, no. 3, pp. 419–422, Aug. 2010.

[11] D. Zhang *et al.*, "Process development and optimization for 3μm high aspect ratio via-middle through-silicon vias at wafer level," *IEEE Trans. Semicond. Manuf.*, vol. 28, no. 4, pp. 454–460, Nov. 2015.

[12] M. Jung, J. Mitra, D. Z. Pan, and S. K. Lim, "TSV stress-aware full-chip mechanical reliability analysis and optimization for 3D IC," *Commun. ACM*, vol. 57, no. 1, pp. 107–115, 2014.

[13] B. Lojek, M. Whiteman, and K. Starzinski, "Alignment mark shift due to thermal non-uniformity: What is moving?" in *Proc. 12th IEEE Int. Conf. Adv. Thermal Process. Semicond. RTP*, Portland, OR, USA, 2004, pp. 150–155.

[14] P. Saettler, M. Boettcher, C. Rudolph, and K.-J. Wolter, "Bath chemistry and copper overburden as influencing factors of the TSV annealing," in *Proc. IEEE 63rd Electron. Compon. Technol. Conf.*, Las Vegas, NV, USA, 2013, pp. 1753–1758.

[15] L. Ji *et al.*, "Effect of annealing after copper plating on the pumping behavior of through silicon vias," in *Proc. IEEE 15th Int. Conf. Electron. Packag. Technol.*, Chengdu, China, 2014, pp. 101–104.

[16] H. He *et al.*, "Influence of thermal annealing on the deformation of Cu-filled TSV," in *Proc. IEEE Electron. Syst.-Integr. Technol. Conf.*, 2014, pp. 1–4.

[17] R. Huang, W. Robl, T. Detzel, and H. Ceric, "Modeling of stress evolution of electroplated Cu films during self-annealing," in *Proc. IEEE. Int. Rel. Phys. Symp.*, Anaheim, CA, USA, 2010, pp. 911–917.

[18] X. Jing *et al.*, "Effect of pre-CMP annealing on TSV pumping in thermal budget and reliability test," in *Proc. IEEE 22nd Int. Symp. Phys. Fail. Anal. Integr. Circuits*, Hsinchu, Taiwan, 2015, pp. 45–47.

[19] J. V. Olmen *et al.*, "Integration challenges of copper through silicon via (TSV) metallization for 3D-stacked IC integration," *Microelectron. Eng.*, vol. 88, no. 5, pp. 745–748, 2011.

[20] S. Ramaswami *et al.*, "Process integration considerations for 300 mm TSV manufacturing," *IEEE Trans. Device Mater. Rel.*, vol. 9, no. 4, pp. 524–528, Dec. 2009.

[21] D. Zhao, T. Wang, Y. He, and X. Lu, "Kinematic optimization for chemical mechanical polishing based on statistical analysis of particle trajectories," *IEEE Trans. Semicond. Manuf.*, vol. 26, no. 4, pp. 556–563, Nov. 2013.

[22] C. Wu *et al.*, "Aggressive diamond characterization and wear analysis during chemical mechanical planarization," *ECS J. Solid State Sci. Technol.*, vol. 2, no. 1, pp. P36–P41, 2013.

[23] Y. Peng, D. Petranovic, and S. K. Lim, "Fast and accurate full-chip extraction and optimization of TSV-to-wire coupling," in *Proc. 51st ACM/EDAC/IEEE Design Autom. Conf. (DAC)*, San Francisco, CA, USA, 2014, pp. 1–6.

[24] Y. Peng, T. Song, D. Petranovic, and S. K. Lim, "On accurate full-chip extraction and optimization of TSV-to-TSV coupling elements in 3D ICs," in *Proc. IEEE/ACM Int. Conf. Comput.-Aided Design (ICCAD)*, San Jose, CA, USA, 2013, pp. 281–288.

[25] B. Lojek, "Low temperature microwave annealing of S/D," in *Proc. 16th IEEE Int. Conf. Adv. Thermal Process. Semicond.*, Las Vegas, NV, USA, 2008, pp. 201–209.

[26] T. Graves-Abe *et al.*, "Novel method for TSV profile metrology using spectral reflectometry," in *Proc. SEMATECH workshop 3D Interconnect Metrol.*, San Francisco, CA, USA, Jul. 2012, pp. 1–19. [Online]. Available: http://www.sematech.org/meetings/archives/3d/10277/pres/2-TSV%20Spectral%20Reflectometry%20IBM%20Nova%20Lam%20-%20Public%20Version.pdf

[27] C. Wu *et al.*, "Pad surface thermal management during copper chemical mechanical planarization," *ECS J. Solid State Sci. Technol.*, vol. 4, no. 7, pp. P206–P212, 2015.

Can Rao received the B.S. degree in mechanical engineering from Tsinghua University, Beijing, China, in 2013.

She is currently pursuing the Ph.D. degree in mechanical engineering with the State Key Laboratory of Tribology, Tsinghua University. Her research interest is on the experiment and modeling of chemical mechanical planarization in 3-D ICs.

Tongqing Wang received the B.S. degree from Jilin University, Changchun, China, in 2006, and the Ph.D. degree in mechanical engineering from Tsinghua University, Beijing, China, in 2012.

He is currently an Associate Research Fellow with the Department of Mechanical Engineering, Tsinghua University. His current research interests include the fundamentals of copper CMP and the development of endpoint detection method in copper CMP.

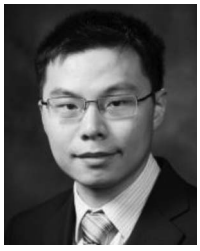

Yarui Peng (S'12) received the B.S. degree from Tsinghua University, Beijing, China, in 2012, and the M.S. and Ph.D. degrees from the School of Electrical and Computer Engineering, Georgia Institute of Technology, Atlanta, USA, in 2014 and 2016, respectively. In 2017, he joined the Department of Computer Science and Computer Engineering, University of Arkansas, as an Assistant Professor.

His research interests are in the areas of computer-aided design, analysis, and optimization for emerging technologies and systems, such as 2.5-D wafer-level-packaging and 3-D ICs, as well as high-efficiency digital designs and memory systems. He is also interested in design automation of high band-gap power electronics and mobile electrified systems. He was a recipient of the Best-in-Session Award in SRC TECHCON 2014 and the Best Student Paper Award in ICPT 2016.

Jie Cheng received the B.S. degree in mechanical engineering from Shandong University, Jinan, China, in 2011, and the Ph.D. degree in mechanical engineering from Tsinghua University, Beijing, China, in 2016.

She is a Research Assistant with the State Key Laboratory of Tribology, Tsinghua University. Her current research interest is chemical mechanical polishing of FinFET structure.

Yuhong Liu received the B.S. degree from the Department of Chemistry, Tsinghua University, Beijing, China, in 2000, and the Ph.D. degree from the CAS Key Laboratory of Molecular Nanostructure and Nanotechnology Institute of Chemistry, Chinese Academy of Sciences in 2005.

She is an Associate Professor with the Department of Mechanical Engineering, Tsinghua University, China. Her current areas of research include nanotribology, nanostructure and nanotechnology of surface and interface, chemical mechanical planarization, and water-based lubrication.

Dr. Liu was a recipient of the Third Prize for the Outstanding Poster in National SPM'8 Conference in 2004, and the Second Prize of China Association for Instrumental Analysis in 2003. She is a member of the International Society of Bionic Engineering, and the International Conference on Electronic Packaging Technology in 2014.

Sung Kyu Lim (S'94–M'00–SM'05) received the B.S., M.S., and Ph.D. degrees from the University of California at Los Angeles in 1994, 1997, and 2000, respectively. In 2001, he joined the School of Electrical and Computer Engineering, Georgia Institute of Technology, where he is currently the Dan Fielder Endowed Chair Professor. His current research interests include modeling, architecture, and electronic design automation for 3-D ICs.

His research on 3-D IC reliability is featured as Research Highlight in the Communication of the ACM in 2014. In 2012, his 3-D IC test chip published in the IEEE International Solid-State Circuits Conference is generally considered the first multi-core 3-D processor ever developed in academia. He has authored the book entitled *Practical Problems in VLSI Physical Design Automation* (Springer, 2008).

Dr. Lim was a recipient of the National Science Foundation Faculty Early Career Development Award in 2006, the Best Paper Awards from the IEEE Asian Test Symposium in 2012 and the IEEE International Interconnect Technology Conference in 2014, and the Class of 1940 Course Survey Teaching Effectiveness Award from Georgia Institute of Technology in 2016. He was on the Advisory Board of the ACM Special Interest Group on Design Automation from 2003 to 2008 and awarded a Distinguished Service Award in 2008. He was an Associate Editor of the IEEE TRANSACTIONS ON VERY LARGE SCALE INTEGRATION (VLSI) SYSTEMS from 2007 to 2009. He has been an Associate Editor of the IEEE TRANSACTIONS ON COMPUTER-AIDED DESIGN OF INTEGRATED CIRCUITS AND SYSTEMS since 2013. He has served on the Technical Program Committee of several premier conferences in EDA.

Xinchun Lu received the B.S. and M.S. degrees in material science and engineering from the Jilin University of Technology, Changchun, China, in 1988 and 1991, respectively, and the Ph.D. degree in material science and engineering from the Institute of Metal Research, Chinese Academy of Sciences in 1994.

He is a Chair Professor of Changjiang Scholars with the Department of Mechanical Engineering, Tsinghua University, China, and the member of the international executive committee of ICPT. His current areas of research include micro-nano fabrication technology, the theory and applications of the micro-nano tribology of the surface and interface, and equipment, and process of chemical mechanical polishing. He has authored or co-authored over 100 journal publications and conference proceedings papers. He holds over 16 patents in the area of CMP equipment.

Dr. Lu was a recipient of the Trans-Century Training Program of the National Ministry of Education, the National Science Found for Distinguished Young Scholars of China, and numerous national awards, including the Award for National Science Development (grade two), and the Science and Technology Advancement Award (grade one), National Ministry of Education.